



How strong are lunar crustal magnetic fields at the surface?: Considerations from a reexamination of the electron reflectometry technique

J. S. Halekas,¹ R. J. Lillis,¹ R. P. Lin,¹ M. Manga,² M. E. Purucker,³ and R. A. Carley⁴

Received 24 September 2009; revised 10 November 2009; accepted 9 December 2009; published 30 March 2010.

[1] Despite extensive study, we do not yet fully understand the origins of the unique lunar crustal magnetism. The strength of surface fields and their relation to local geology are crucial pieces of the puzzle. However, only a few surface measurements exist, and spacecraft magnetometers cannot detect magnetization with wavelengths much smaller than the orbital altitude. Meanwhile, electron reflectometry (ER) enables a remote measurement of surface fields, but its sensitivity to magnetization with different spatial scales is not well understood. In this paper, we report on new simulations of the ER technique and its sensitivity to magnetic fields produced by simulated crustal magnetization with various strengths and spatial distributions, utilizing full particle tracing simulations and the same data analysis techniques used for space data. We find that the ER technique reliably detects surface fields from magnetization with wavelengths larger than ~ 10 km but has increasingly less sensitivity to smaller wavelengths. Since the few surface measurements we have imply very incoherent near-surface magnetization, this implies that the ER technique may seriously underestimate the strength of lunar fields in some areas. Our results imply that small-scale impact-related crustal magnetization may prove even more important than previously thought.

Citation: Halekas, J. S., R. J. Lillis, R. P. Lin, M. Manga, M. E. Purucker, and R. A. Carley (2010), How strong are lunar crustal magnetic fields at the surface?: Considerations from a reexamination of the electron reflectometry technique, *J. Geophys. Res.*, 115, E03006, doi:10.1029/2009JE003516.

1. Introduction

[2] Since its surprising discovery in the Apollo era, lunar crustal magnetism has proven enigmatic and difficult to interpret. Though the Moon does not currently have an active core dynamo, we now know that it has extensive, though weak, remanent crustal magnetization. The magnetic fields resulting from this magnetization were first measured by surface magnetometers at the Apollo 12, 14, 15, and 16 landing sites [Dyal *et al.*, 1974] and by magnetometers and electron reflectometer experiments on the Apollo 15 and 16 subsatellites [Coleman *et al.*, 1972; Anderson *et al.*, 1975; Lin, 1979]. More recently, the Lunar Prospector Magnetometer/Electron Reflectometer (LP MAG/ER) experiment mapped out the distribution of these fields in more detail [Halekas *et al.*, 2001; Hood *et al.*, 2001; Mitchell *et al.*, 2008].

[3] However, despite extensive study, the origins of lunar crustal magnetization remain unknown and controversial. Early experiments conducted on returned samples suggested that some had a primary thermal remanence, implying the presence of a strong magnetizing field from ~ 3.9 to ~ 3.6 Gyr ago [Fuller and Cisowski, 1987], thus arguing for the existence of an ancient lunar dynamo during this time period. Recent investigations of the samples have complicated the picture, with one experiment suggesting the existence of an even more ancient dynamo [Garrick-Bethell *et al.*, 2009] and another calling into question the existence of a “magnetic era” [Lawrence *et al.*, 2008].

[4] The central magnetic anomalies found in some impact basins also suggest thermal remanence in a steady magnetizing field, though shock remanence in the central uplift could also potentially explain them [Halekas *et al.*, 2003]. On the other hand, the apparent association of much of the strong crustal magnetization with basin ejecta [Halekas *et al.*, 2001; Hood *et al.*, 1979, 2001] or the antipodes of young large impact basins [Mitchell *et al.*, 2008] suggests an origin involving shock remanent magnetization formed by transient impact processes, perhaps obviating the need for an ancient dynamo.

[5] Whatever their origins, we observe lunar crustal magnetic fields widely and nonuniformly distributed over the lunar surface, with some strongly magnetic regions ex-

¹Space Sciences Laboratory, University of California, Berkeley, California, USA.

²Department of Earth and Planetary Sciences, University of California, Berkeley, California, USA.

³Planetary Geodynamics Laboratory, NASA Goddard Space Flight Center, Greenbelt, Maryland, USA.

⁴Grant Institute of Earth Science, University of Edinburgh, Edinburgh, UK.

tending for up to hundreds of kilometers. For even these largest source regions, however, magnetic field polarities vary over spatial scales down to the limit of the measurements, suggesting a significant, or even dominant, small-wavelength component to the crustal magnetization. Surface magnetometers at the Apollo 14 and 16 landing sites measured fields that vary dramatically in direction and magnitude over kilometer scales [Dyal *et al.*, 1974], supporting this inference.

[6] The crucial pieces of information needed to determine the origins of lunar remanent crustal magnetization are its strength and its relationship to surface and subsurface geology. However, these prove surprisingly difficult to determine, especially for very incoherent magnetization. Of course, relating magnetic field measurements to subsurface magnetization strength is inherently a nonunique problem. Nonetheless, if we knew both the strength and spatial distribution of crustal magnetic fields, we could make reasonable estimates of the magnetization strength and distribution. Unfortunately, though, we cannot even easily determine the distribution of crustal magnetic field strength near the surface. Surface magnetometer measurements provide ground truth but only exist for a few landing sites. Spacecraft magnetometers have mapped much of the lunar crustal magnetic field distribution, but the observation altitude of tens of kilometers or more limits the resolvable wavelength, rendering estimates of total surface field strength impossible for magnetization with significant small-wavelength components. Electron reflectometry (ER) measurements, finally, provide a remote measurement of the surface field strength, seemingly overcoming this difficulty; however, the ER technique is also potentially limited by the gyrodiameter of the electrons used to probe the field.

[7] If the small-wavelength component of lunar crustal magnetization proves as important everywhere as suggested by the few surface measurements, this could indicate that current maps of lunar crustal magnetic fields significantly underestimate the surface field magnitude (and thus, most likely, the strength of the magnetization). Recent measurements of very strong but spatially incoherent (centimeter-scale) magnetization in the Vredefort crater [Carporzen *et al.*, 2005], over which aeromagnetic maps show very weak fields, provide an example of just such a case at the Earth. If crustal magnetization with very small spatial scales actually dominates in some areas of the Moon (especially if it does so only in certain lunar geologic regions), one might easily reach very erroneous conclusions about the likelihood and/or importance of different origin scenarios for lunar magnetism.

[8] The response of a magnetometer to distributions of magnetization with different spatial wavelengths is well understood and easily modeled; however, no one has yet considered the analogous response of the ER technique. Therefore, in this paper we simulate the response of an ER experiment like that on LP to distributions of crustal magnetization with different strengths and spatial wavelengths and consider the implications of our results for lunar magnetism and its origins.

2. Electron Reflectometry

[9] The ER technique, first discovered serendipitously by experiments on the Apollo subsatellites, relies on the mag-

netic mirror effect. Absent magnetic field gradients or electric fields, most incident electrons impact the Moon, with only a small backscattered population. Above regions with crustal magnetic fields, though, some electrons reflect before reaching the surface, and a spacecraft on an orbit intersecting field lines that connect to the lunar surface will measure a reflected population of electrons traveling away from the Moon in addition to the incident population traveling toward the surface.

[10] Assuming magnetic field scale sizes large in comparison to electron gyroradii and no dynamics other than those on time scales long compared to the electron gyroperiod (in other words, adiabatic behavior), we can easily treat electron motion. In this case, electrons travel in helical paths along magnetic field lines, preserving their energy and magnetic moment $\mu = mv_{\perp}^2/(2B) = mv^2 \sin^2 \alpha/(2B)$, where the pitch angle α is defined as the angle between electron velocity and magnetic field and B is the magnetic field magnitude. If electrons travel through a positive magnetic field gradient, the pitch angle therefore must rotate toward 90° in order to preserve the magnetic moment. If the pitch angle reaches 90° before the electron impacts the surface, it reflects; this forms the basis of the magnetic mirror effect. The electron reflection process depends on the initial pitch angle of the electron, with more field aligned electrons being more difficult to reflect. Thus, one observes reflected electrons with pitch angles less field aligned, but none with pitch angles more field aligned, than a cutoff pitch angle α_c , where $\sin^2 \alpha_c = B/B_m$, with B_m being the total field magnitude at the surface.

[11] A measurement of α_c , along with spacecraft magnetic field data, therefore enables a determination of the total surface field. In order to find the crustal field magnitude B_c , one then must subtract the ambient field from this total surface field. (The ER technique assumes vacuum superposition of ambient and crustal fields; thus, we only use ER in regions with low plasma densities, such as the lunar wake and terrestrial magnetotail.) Assuming an ambient (i.e., noncrustal) magnetic field homogenous over scales comparable to or larger than the orbital altitude and a small crustal field component at the spacecraft, we can use the field B measured at the spacecraft for this subtraction. Unfortunately, one cannot perform an exact subtraction because of the vector nature of the superposition of ambient and crustal fields and the scalar nature of the reflectometry measurement. Mathematically, $B_c = |\mathbf{B}_m - \mathbf{B}| \geq B_m - B$; therefore, the ER technique can only provide a lower limit for the magnitude of the crustal field. Depending on the relative magnitudes and orientations of B and B_c , this lower limit may or may not prove a good approximation to the actual value of B_c ; for some cases it can even return a crustal field estimate of zero (but not a negative field estimate). Despite this limitation, the ER technique provides a simple way to remotely estimate the crustal field magnitude at the surface, requiring only local measurements of the magnetic field and electron angular distribution.

[12] If one cannot make an accurate measurement of the cutoff pitch angle, one can instead measure the total reflected flux and compare it to the incident flux in order to determine the so-called reflection coefficient. For an isotropic distribution and ignoring backscatter from the surface, this reflection coefficient is simply $R = |\cos \alpha_c|$, allowing

one to use the mathematical formulation presented above equally well to determine the surface field from a measurement of R . Unfortunately, one can only reliably use the reflection coefficient in cases with a roughly isotropic incident electron population. Despite this limitation, reflection coefficient data from the Apollo subsatellites (which had limited angular resolution) still allowed impressively accurate mapping of the lunar crustal field distribution [Anderson *et al.*, 1975; Lin, 1979]. More recently, the LP ER instrument, which had excellent angular resolution, allowed accurate and precise measurements of the cutoff pitch angle and enabled the use of the reflectometry technique without the assumption of electron isotropy [Halekas *et al.*, 2001; Mitchell *et al.*, 2008].

[13] Conceptually, the ER technique proves simple and straightforward; however, in practice several factors can complicate the analysis. First, electric fields, as well as magnetic field gradients, can act to reflect electrons. Luckily, by utilizing measurements at multiple energies, one can extend the ER technique to simultaneously measure both crustal magnetic fields and near-surface electric fields [Anderson *et al.*, 1975; Mitchell *et al.*, 2008]. Data analysis for cases with electric fields proves completely analogous (other than the requirement of multiple energy channels) to that for cases with only magnetic fields, so we neglect electric field effects in this paper.

[14] Nonadiabatic electron motion proves potentially more problematic for the ER technique. Strictly speaking, the ER formulation described above only remains valid while the adiabatic assumption holds. Unfortunately, since lunar crustal fields have significant components at wavelengths smaller than the gyroradius of the electrons used for ER measurements, we cannot blindly rely on the adiabatic assumption. Encouragingly, simulations of electron trajectories above a buried dipole suggest that the adiabatic formulation still provides a good first approximation to the ER response [Anderson *et al.*, 1975]. However, no one has yet modeled the ER response to arbitrarily complicated distributions of magnetization or parameterized the ER technique's sensitivity to magnetic fields produced by crustal magnetization with different strengths and spatial wavelengths. In this paper, we therefore investigate the response of the ER technique by simulating electron trajectories above various crustal magnetization distributions, generating synthetic ER data sets that we can analyze just as we would real ER data and considering the results as a function of crustal magnetization parameters.

3. Simulation Results

3.1. Generating Realistic Magnetic Field Distributions

[15] Previous simulations of the response of the ER technique used relatively simple source distributions consisting of buried dipoles [Anderson *et al.*, 1975]. While this allowed a basic understanding of the ER response, in this work we wish to understand the sensitivity of the ER technique as a function of the spatial wavelength of crustal magnetization; therefore, we use more complicated synthetic magnetization distributions. In order to generate these distributions, we use a simple Fourier method (assuming periodic boundary conditions in x , y , and z) similar to that used for some previous terrestrial studies [Pilkington and

Todoschuck, 1993]. We generate a completely random (white noise) three-dimensional distribution of magnetization, transform to the wave number domain, multiply by an appropriate filter in order to select magnetization in a particular wavelength range or to generate a power law distribution of magnetization, and then transform back to the spatial domain. No matter what the form of the original random distribution, this procedure generates magnetization with the specified spatial wavelengths and with a nearly Gaussian distribution. (One can use an iterative procedure to generate magnetization with a non-Gaussian distribution [Kantelhardt, 2009]; we have found that our results do not depend sensitively on the form of the strength distribution, so we opt to use the simplest form, resulting in a Gaussian magnetization strength distribution centered on zero.)

[16] We produce three-dimensional magnetization distributions with a thickness of 32 km (a physically reasonable value for the Moon), a spatial extent of $128 \times 128 \text{ km}^2$, and a grid spacing of 0.5 km. Thus, we only consider magnetization with wavelengths of 1 km or larger in this paper. We will find that the ER technique has very little sensitivity to even kilometer-scale magnetization, so we lose little by neglecting smaller wavelengths.

[17] We construct distributions of magnetization with each of three orthogonal directions. In the end, we find similar results for all magnetization directions but still consider all three separately, finally averaging the three response functions we calculate to get an average ER response to magnetization with an arbitrary direction. We opt for this method since the magnetic morphology can depend on the magnetization direction (for magnetization in the vertical direction, more field lines escape the crust, leading to stronger magnetic fields and different topologies), so the ER response could also potentially depend on magnetization direction.

[18] Once we generate a crustal magnetization distribution, we calculate the vector magnetic field distribution above this magnetization. We again use a Fourier method (assuming periodic boundary conditions in x and y), as described by *Blakely* [1996]. We calculate the magnetic field on a three-dimensional grid, extending from the surface to 32 km altitude, again with 0.5 km resolution (sufficient for accurate electron trajectory calculations). We then normalize this magnetic field distribution to have a specified average magnitude at the surface. Figure 1 shows a sample distribution generated by the procedures described above, with an average surface magnetic field magnitude of 10 nT.

3.2. Simulating Electron Reflectometer Data

[19] After we construct a magnetic field distribution above synthetic crustal magnetization with the desired properties, we trace electron trajectories through these fields, with a 10 nT vertical background field added to the crustal field distribution (corresponding to a typical ambient solar wind or magnetospheric field). We launch electrons from a spacecraft altitude of 32 km, with a kinetic energy of 220 eV (one of the three main energy channels used for LP ER analysis), an isotropic downward initial velocity distribution, and random starting locations evenly distributed between $x, y = \pm 40 \text{ km}$. (This grid is smaller than the magnetic field grid, which thus avoids most trajectories that pass near the edges of the grid; a few test simulations with larger grids

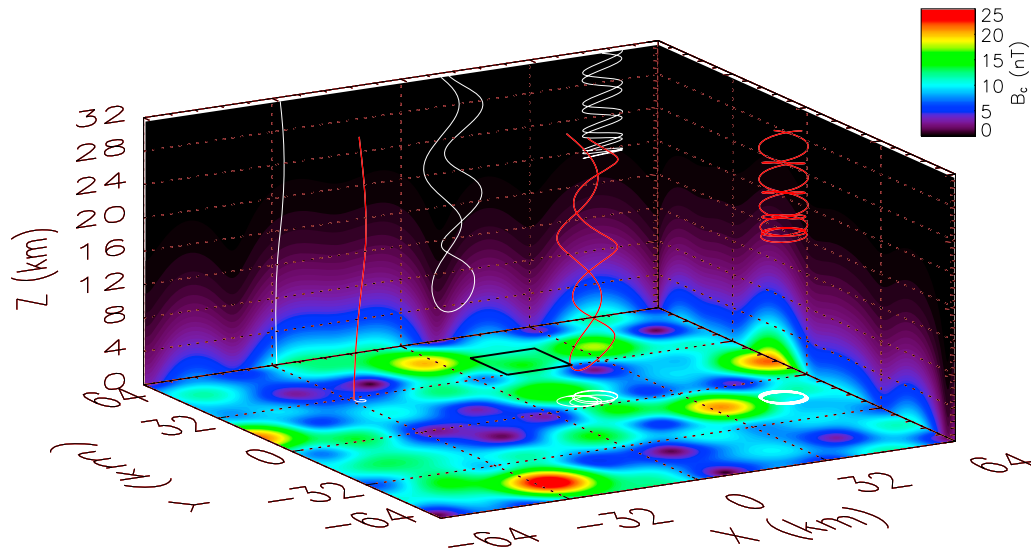


Figure 1. Model magnetic fields above a crustal magnetization distribution with a spatial wavelength of 32 km, with field magnitudes shown in color for the $z = 0$, $x = 64$, and $y = 64$ planes. Red traces show sample electron trajectories through these fields (with a background field of 10 nT in the z direction), with white traces for the projections of these trajectories on the $z = 0$ and $y = 64$ planes. The black box indicates the x - y region considered in Figure 2.

show that this practice ensures negligible edge effects.) We trace electrons using a fourth-order Runge-Kutta integration method with an adaptive time step, with each spatial step constrained to be smaller than both one fiftieth of a gyro-circumference and 0.25 km. In practice, this results in conservation of energy to better than one part in 10^4 . We follow electrons until they strike the surface, magnetically reflect and return to spacecraft altitude of 32 km, or leave the simulation box. We show three sample trajectories in Figure 1 for one electron that reaches the surface and for two that reflect before reaching the surface.

[20] For each simulation, we launch 10^5 electrons and calculate the ER response in sixty-four 4×4 km² regions, evenly tiling the area between x , $y = \pm 32$ km (smaller than the launch region, thus again eliminating most edge effects). The simulated electron distribution for each given region therefore has a few hundred electrons, minimally sufficient to determine the reflected pitch angle distribution but providing similar statistics to those often achieved in space. To calculate the ER response, we then proceed exactly as in the analysis of space data [Halekas et al., 2001; Mitchell et al., 2008] from the LP ER experiment. We first create pitch angle distributions by binning the reflected electrons' final pitch angles into 11.25° angular bins (the same as the LP ER instrumental resolution). We then oversample the resulting distribution and fit to a step function in order to determine the cutoff pitch angle α_c . Finally, we calculate the ER estimate of the crustal field as $\tilde{B}_c \geq B/\sin^2 \alpha_c - B$. In Figure 2, we show an illustrative loss cone fit (this test case has a different number of trajectories and a larger sample region than our typical model run) for a region above the magnetic field configuration of Figure 1. The cutoff pitch angle of 44° determined for this distribution, for a 10 nT field at spacecraft altitude, gives us a crustal field estimate of 10.7 nT, close to the actual average surface magnetic field magnitude of 12.5 nT in the selected region.

3.3. Characterizing the Sensitivity of the Electron Reflectometry Technique

[21] In Figure 3, we show the average ER response from 384 simulation runs conducted as described in section 3.2, consisting of two runs each for cases with crustal magnetization in three orthogonal directions, for eight different spatial wavelengths from 1 to 128 km and for eight different average surface magnetic field strengths from 1 to 200 nT (both roughly logarithmically spaced). We choose a maximum field of 200 nT since fields much larger than this produce an expected loss cone angle so small that we cannot generally measure it. We normalize all values by the actual average crustal field magnitude; thus, a perfect ER mea-

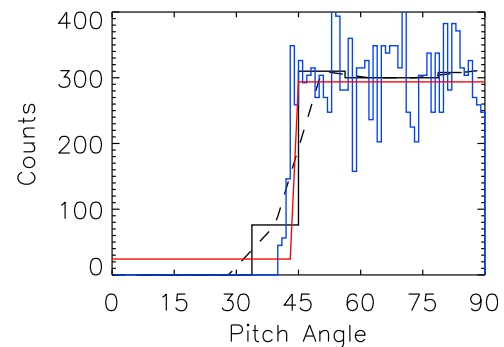


Figure 2. Model reflected electron fluxes as a function of pitch angle, as measured at 32 km altitude, for the region outlined in Figure 1. The blue histogram shows electron data (arbitrary units) binned at 1° resolution. The solid black histogram shows the same data binned at the 11.25° resolution of the LP ER instrument. The dashed black line shows the same distribution oversampled at 1° resolution. Red line shows the best step function fit to the oversampled distribution, indicating a cutoff pitch angle of 44° .

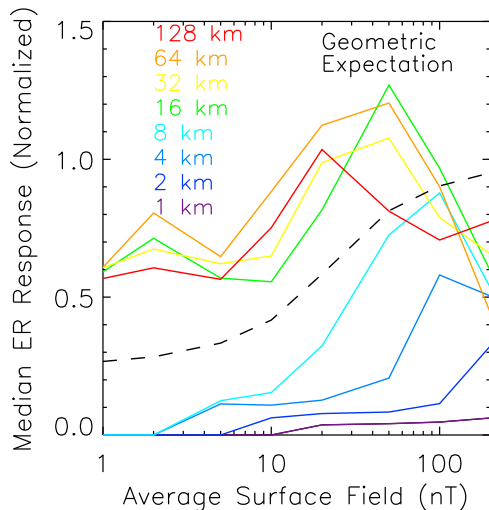


Figure 3. Modeled electron reflectometer response (normalized by actual surface field) to random crustal magnetization distributions with eight different spatial wavelengths, each for eight different average surface magnetic field strengths. Each data point represents an average over six model runs, two for each of three orthogonal magnetization directions. The dashed line shows the expected ER response based on purely geometric considerations (neglecting deflection of trajectories around crustal field regions), averaged over all possible relative orientations of ambient and crustal magnetic fields.

surement would return unity for all cases. We parameterize by the measurable quantity of average surface magnetic field rather than magnetization strength. One should note that the average surface field is proportional to magnetization intensity for magnetization with a given wavelength but not for magnetization with different wavelengths. Our simulations have proven very repeatable, with nearly the same average ER response (almost always within $\sim 10\%$) for the same conditions but different initial random distributions of magnetization, even for cases with spatial wavelength comparable to the size of the simulation region.

[22] We found the determination of cutoff pitch angles near 90° rather unreliable in our simulations since the electron population with pitch angles near 90° is not always evenly sampled in our simulation and since we only consider the reflected half of the electron distribution in our analysis. Accordingly, for the purposes of this study, we arbitrarily set any average crustal field estimates below 0.55 nT to zero; this only affects a few data points in Figure 3.

[23] We can explain much of the form of the ER response shown in Figure 3 in terms of the approximation necessarily introduced in the ER technique by using a scalar subtraction of the ambient field from the total surface field as an estimate of the vector subtraction one would need to accurately isolate the crustal field component (as described in section 2). This approximation leads to different levels of inaccuracy for different relative orientations and magnitudes of crustal versus ambient magnetic fields. For any crustal field, we can determine the average expected response of the ER technique purely on the basis of geometric considerations by integrating the ER crustal field estimator over all relative

orientations of ambient and crustal field (for an assumed ambient field of 10 nT). We show this theoretical curve (normalized) in Figure 3 and note that the general trend of the simulation results does indeed follow this expected form. On average, the ER estimate has higher fidelity for larger crustal fields since the removal of the ambient field introduces only a small perturbation.

[24] However, this simple calculation does not take into account the curvature of magnetic field lines. As described by *Anderson et al.* [1975], magnetic field lines bend toward regions with parallel ambient and crustal fields and away from regions with antiparallel ambient and crustal fields. Thus, electron trajectories, which spiral along magnetic field lines, tend to deflect toward regions with higher total surface fields, and we therefore expect an average crustal field estimate from the ER technique somewhat higher than the theoretical curve purely on the basis of geometric considerations. Indeed, the simulation results for crustal magnetization with wavelengths larger than the electron gyroradius (for 220 eV electrons in a 10 nT field, the gyroradius is 10 km) do tend to lie above the dashed curve in Figure 3.

[25] The general trend of the simulation results shown in Figure 3 indicates that the ER technique has more sensitivity to crustal magnetization with larger wavelengths for any surface field strength. We could have expected this since larger wavelengths correspond to larger magnetic field scale heights (that is, crustal fields comparable to the ambient field extend to higher altitudes) and electrons have longer to “sense” the crustal field before impacting the surface. For the smallest wavelengths of crustal magnetization, significant crustal fields extend less than one electron gyroradius above the surface, leading to essentially completely nonadiabatic scattering and less efficient electron reflection.

[26] For the smallest crustal magnetic fields ($< \sim 10$ nT), the two effects described in the preceding paragraphs essentially characterize the ER response. For these weak fields, we observe a clear dichotomy between crustal magnetization with spatial wavelengths larger than and smaller than the nominal electron gyroradius of ~ 10 km. For magnetization wavelengths larger than the gyroradius, the ER measurement behaves as expected on the basis of the approximations implicit in the technique, given some additional focusing of electron trajectories into regions with parallel ambient and crustal fields. For wavelengths smaller than the gyroradius, on the other hand, the ER technique proves less sensitive than expected on the basis of adiabatic theory because of the essentially nonadiabatic scattering of electrons from crustal fields localized near the surface.

[27] For somewhat larger crustal fields (~ 10 – 50 nT), this distinction becomes less pronounced both because larger field magnitudes locally reduce the electron gyroradius and because crustal fields comparable to the ambient field extend to higher altitudes. Somewhat surprisingly, for these medium fields the ER response can exceed unity for large magnetization wavelengths because of the efficient focusing of electron trajectories into cusps with strong crustal fields parallel to the ambient field.

[28] For the largest crustal fields ($> \sim 50$ nT), the ER response rolls off, especially for larger magnetization wavelengths. Nonadiabatic scattering at least partially explains this decreased sensitivity. For these large fields, we expect

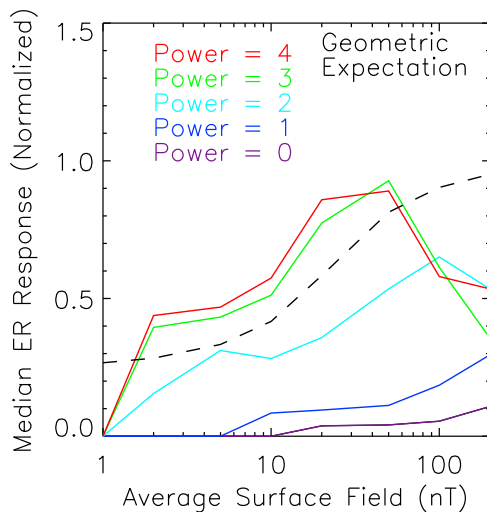


Figure 4. Modeled normalized ER response to random crustal magnetization distributions with a power law distribution of spatial wavelengths (i.e., $|M_k|^2 \propto k^{-\beta}$) for five different spectral powers β , with each data point representing six model runs as in Figure 3. Dashed line is the same as in Figure 3.

to observe a cutoff pitch angle near zero. Electrons with small (field-aligned) pitch angles, when encountering significant field line curvature, can easily scatter to larger pitch angles. Our simulations show that this nonadiabatic behavior broadens the loss cone and makes its boundary less sharp, producing smaller crustal field estimates. This effect appears most pronounced for the largest fields and largest magnetization wavelengths since for these cases significant crustal fields (and thus field line curvature) extend to the highest altitudes. The reduction of the electron gyrodiometer by stronger fields should mitigate this effect to some degree, but it appears that nonadiabatic effects still prevail in this regime, rendering ER results for the strongest fields unreliable.

[29] We note several other reasons to treat ER estimates for these strong fields with care. At the spacecraft altitudes considered here, the strongest crustal fields produce mostly closed magnetic field lines. Thus, ambient plasma may have little access to these field lines, reducing the applicability of the ER technique, which cannot work without a source population of electrons. In addition, the large field line curvature above these regions leads to inaccurate extrapolation of the foot point of the magnetic field line and therefore mapping errors on the order of the spacecraft altitude or larger. Luckily, orbital magnetometer measurements efficiently detect crustal magnetization with large wavelengths and large field strengths. The magnetic field produced by magnetization with a given spatial wavelength falls off with altitude as $B(z) \propto e^{-kz}$ [Blakely, 1996], so a magnetometer has very limited sensitivity to magnetization with spatial wavelengths smaller than the orbital altitude (much less than the ER technique, whose limited efficiency at measuring crustal magnetization with small wavelengths we have shown in this study). However, for wavelengths larger than the orbital altitude, especially for strong crustal magnetic fields, a magnetometer measurement clearly has

many advantages over the ER technique. Thus, ER and magnetometer measurements prove complementary in many cases.

[30] The actual lunar crustal magnetization likely has significant components at multiple wavelengths rather than at only a single wavelength. Many geophysical quantities, including terrestrial crustal magnetization [Pilkington and Todoeschuck, 1993], have been shown to have a distribution of spatial wavelengths that follows fractal, or power law, scaling. Therefore, we conducted another set of simulations for crustal magnetization with power law distributions of spatial wavelengths for five different power law exponents and show the results in Figure 4. By and large, these simulation results hold few surprises. The form of the ER response still generally hews to the expectations from an adiabatic treatment, but because of nonadiabatic effects, the ER technique much less efficiently detects magnetic fields produced by crustal magnetization distributions with smaller power law scaling exponents (in other words, those with more significant components at smaller wavelengths), as expected from the results presented above.

4. Lunar Magnetic Fields

[31] We see from the results presented in Figures 3 and 4 that crustal magnetization with different spatial wavelengths can lead to very different ER responses. Unfortunately, this implies that existing ER estimates could correspond to lunar surface crustal magnetic fields with rather different strengths than those heretofore assumed, especially for cases in which crustal magnetization at small wavelengths dominates. Indeed, our simulations demonstrate that we cannot, in general, uniquely relate LP ER measurements to surface magnetic field strengths without more information about the spatial wavelength or wavelengths of lunar crustal magnetization.

[32] Unfortunately, even if its spatial components do indeed follow simple fractal scaling, we cannot easily determine a power law exponent for lunar crustal magnetization. One might guess that crustal magnetization on the Moon should scale like that on the Earth, where typical crustal magnetic fields have 2-D power spectra with a power law exponent of ~ 3 , corresponding to a 3-D magnetization distribution with a power law exponent β of ~ 4 [Pilkington and Todoeschuck, 1993]. Alternatively, one could extrapolate from the magnetic field power spectrum determined from LP MAG data, which appears essentially flat (white) at large wavelengths [Purucker, 2008]. Unfortunately, we can only rely on the MAG power spectrum up to $\sim 150^\circ$ (corresponding to wavelengths of ~ 70 km); however, we could reasonably guess that this essentially flat power spectrum should continue out to higher degrees. If so, we would expect a 3-D magnetization distribution with a power law exponent β of ~ 1 [Maus and Dimri, 1994]. These two power law cases would lead to very different small-scale surface magnetic field distributions and very different ER sensitivities, and we cannot easily determine which one (if either) actually exists on the Moon.

[33] In an attempt to place further constraints on this problem, we compare LP ER and MAG data, as well as the few surface magnetometer measurements available. In Figure 5, we show LP ER and MAG magnetic field mag-

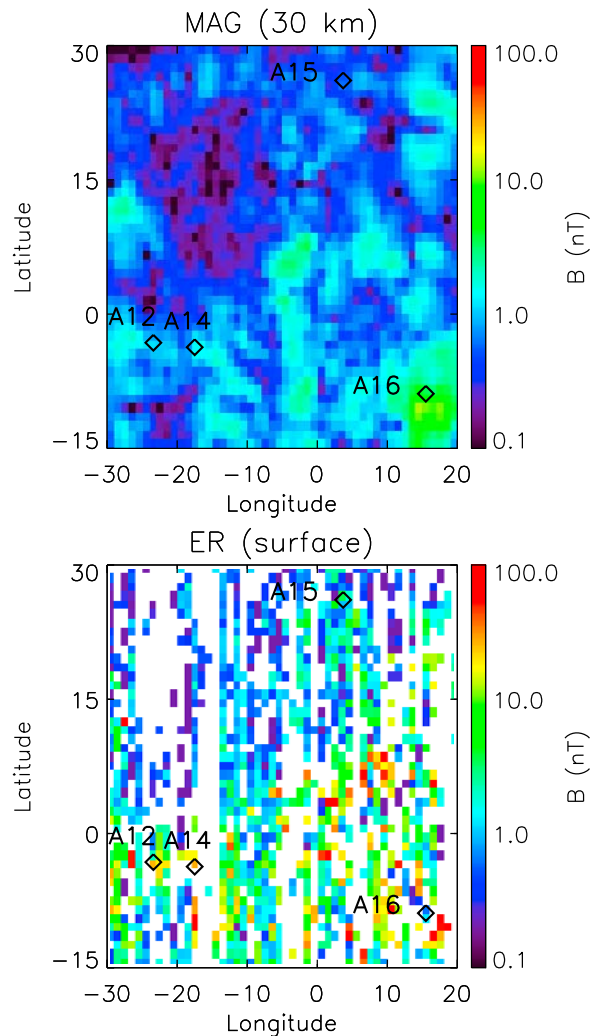


Figure 5. Crustal magnetic field magnitude at 30 km altitude (from *Purucker's* [2008] spherical harmonic model, based on LP MAG measurements) and at the surface (from LP ER measurements, binned at 1° resolution), with locations of Apollo surface magnetometer measurements.

nitude maps over a region of the nearside that covers several Apollo landing sites. We processed the ER data just as we did our simulation data (except that we used measurements at multiple energies to correct for electric field effects, as described by *Mitchell et al.* [2008]), in order to determine a lower limit to the surface crustal magnetic field magnitude, and averaged the resulting estimates into 1° spatial bins. The magnetometer map, meanwhile, shows a spherical harmonic representation of LP MAG data (calculated at 30 km altitude), which uses an innovative cross-correlative technique to isolate crustal fields [*Purucker*, 2008]. We also indicate the locations of the four Apollo landing sites that had surface magnetometer measurements [*Dyal et al.*, 1974].

[34] By and large, the ER and magnetometer maps show the same distribution of crustal magnetic fields, though the ER map has much less complete coverage and shows much stronger fields (as expected since the ER estimates the surface field rather than that at altitude). Both maps show that the Apollo 12 and 14 landing sites lie in regions with

moderate crustal fields, the Apollo 15 landing site lies in a weakly magnetic region, and the Apollo 16 landing site lies just north of one of the strongest magnetic features on the nearside (the Descartes anomaly, first recognized by *Halekas et al.* [2001]).

[35] Table 1 shows the surface field estimated from the LP ER data, the range of surface fields measured by surface magnetometers, and the field at 30 km altitude from the LP MAG data for each of the Apollo landing sites. For the Apollo 12 and 15 sites, the LP ER estimate lies reasonably close to the actual surface field measured by the surface magnetometers, suggesting spatial wavelengths of tens of kilometers or more for the local crustal magnetization. At both of these sites, we only have surface magnetometer measurements for one location, so we have no independent estimate of the spatial characteristics of the local crustal magnetization. At the Apollo 14 and 16 sites, on the other hand, surface magnetometer measurements from different locations show fields that vary dramatically in both polarity and magnitude over scales of a few kilometers, implying commensurately small dominant wavelengths for the local crustal magnetization. Consistent with a small magnetization wavelength, the ER technique underestimates the average surface field for both of these sites, dramatically so for the Apollo 16 site (though this could result at least partially from magnetic curvature and mapping location errors due to the proximity of the very strong Descartes anomaly). Also consistent with a more significant small-wavelength component, the Apollo 14 and 16 sites show the greatest reduction from the peak magnetic field measured at the surface to the field measured at 30 km altitude. For all four sites, LP MAG data show such a significant reduction in field strength from the surface to 30 km altitude that one would find it very difficult to use spacecraft magnetometer data to obtain a quantitative estimate of the surface field magnitude.

5. Conclusions and Implications

[36] In the end, we can draw several general conclusions from the work described in this paper. First, small spatial wavelengths of crustal magnetization clearly dominate at some lunar surface locations, and our simulations show that the ER technique will significantly underestimate the magnitude of the surface fields in these areas. Therefore, we must take great care in interpreting ER estimates of surface crustal magnetic field magnitudes. Second, the dominant spatial wavelength of crustal magnetization likely varies over the lunar surface since the ER technique does accurately measure the surface field at a few sites. Therefore, we must also take great care in comparing ER estimates for different locations and different geologic formations since

Table 1. Measured Fields at Apollo Sites

	Surface Field (nT)	Wavelength ^a	ER Estimate (nT)	Field at 30 km (nT)
Apollo 12	38	NA	26	1.2
Apollo 14	43–103	A few km or less	27	1.5
Apollo 15	3.4	NA	3.5	0.5
Apollo 16	112–327	A few km or less	0.6	3.5

^aNA means not available.

they might have quite different magnetization characteristics and the ER technique might therefore have very different sensitivities. Finally, magnetometer measurements provide the only unbiased estimate of crustal magnetic field strengths. However, orbital measurements cannot resolve small-wavelength components. Therefore, to fully characterize the lunar crustal magnetization distribution, surface measurement likely remains the only reliable technique.

[37] The variable ER response to magnetization with different spatial wavelengths implies that we may have underestimated the strength of the surface crustal field, especially in regions with a dominant small-wavelength magnetization component. In general, one would expect the magnetization produced by thermal remanence in a dynamo field to be relatively coherent since large volumes of cooling material can take on a magnetic remanence in the same direction as the dynamo field. On the other hand, we would tend to expect magnetization produced by impact processes to have less spatial coherence. Thus, ER maps may actually underestimate the importance of impact-related processes (though we already consider these very important). Supporting this inference, the two Apollo landing sites that appear to have the least spatially coherent magnetization roughly coincide with basin ejecta, with the Fra Mauro formation at Apollo 14 likely being formed by Imbrium ejecta and the Descartes formation near Apollo 16 most likely being formed by Nectaris ejecta. Apollo and LP data do indicate significant crustal fields above both of these formations [Hood *et al.*, 1979; Halekas *et al.*, 2001], but the comparisons described above show that we may have underestimated the strength of this apparently ejecta-associated magnetism. Thus, our results support a picture of spatially incoherent crustal magnetization associated with impact ejecta, underestimated by the ER technique, and poorly resolved by orbital magnetometer measurements, which would imply that impact processes could play an even more important role in lunar magnetism than previously thought.

[38] Finally, we consider the implications of our results for the lunar surface crustal magnetic field strength. Given ER estimates of surface fields of up to hundreds of nanotesla, the existence of magnetization with kilometer-scale wavelengths in at least a few locations, and the low sensitivity of the ER technique to spatially incoherent magnetization demonstrated in this paper, it seems likely that surface field strengths could reach thousands of nanotesla in some locations. For very spatially incoherent magnetization (subkilometer-scale wavelengths), fields could conceivably reach even higher values. If true, these stronger than expected surface fields could have interesting implications for sample magnetization. Some samples that show magnetization consistent with thermal remanence could have acquired their remanence by cooling in a field produced by strong local crustal magnetization (possibly generated by shock) rather than in a dynamo field. Such a mechanism cannot likely explain the most strongly magnetized samples (though at least some of these might, in the end, prove to have shock rather than thermal remanence), but it could conceivably explain the magnetization in the sample recently analyzed by Garrick-Bethell *et al.* [2009], which indicated a thermal remanence acquired in an ancient field on the order of 1000 nT. Thus, again, our results suggest

that lunar crustal magnetization resulting from nondynamo processes may prove more important than previously thought.

[39] **Acknowledgments.** We gratefully acknowledge numerous conversations about the origins of lunar magnetism with Mike Fuller and Lon Hood. This work was supported by NASA grant NNX07AN94G.

References

- Anderson, K. A., R. P. Lin, R. E. McGuire, and J. E. McCoy (1975), Measurement of lunar and planetary magnetic fields by reflection of low energy electrons, *Space Sci. Instrum.*, *1*, 439–470.
- Blakely, R. J. (1996), *Potential Theory in Gravity and Magnetic Applications*, Cambridge Univ. Press, Cambridge, U. K.
- Carporzen, L., S. A. Gilder, and R. J. Hart (2005), Palaeomagnetism of the Vredefort meteorite crater and implications for craters on Mars, *Nature*, *435*, 198–201, doi:10.1038/nature03560.
- Coleman, P. J., B. R. Lichtenstein, C. T. Russell, L. R. Sharp, and G. Schubert (1972), Magnetic fields near the Moon, *Geochim. Cosmochim. Acta*, *36*, 2271–2286.
- Dyal, P., C. W. Parkin, and W. D. Daily (1974), Magnetism and the interior of the Moon, *Rev. Geophys.*, *12*, 568–591, doi:10.1029/RG012i004p00568.
- Fuller, M., and S. M. Cisowski (1987), Lunar paleomagnetism, in *Geomagnetism*, edited by J. Jacobs, pp. 307–455, Academic, Orlando, Fla.
- Garrick-Bethell, I., B. P. Weiss, D. L. Shuster, and J. Buz (2009), Early lunar magnetism, *Science*, *323*, 356–359, doi:10.1126/science.1166804.
- Halekas, J. S., D. L. Mitchell, R. P. Lin, S. Frey, L. L. Hood, M. H. Acuña, and A. B. Binder (2001), Mapping of crustal magnetic anomalies on the lunar near side by the Lunar Prospector electron reflectometer, *J. Geophys. Res.*, *106*, 27,841–27,852, doi:10.1029/2000JE001380.
- Halekas, J. S., R. P. Lin, and D. L. Mitchell (2003), Magnetic fields of lunar multi-ring impact basins, *Meteorit. Planet. Sci.*, *38*, 565–578, doi:10.1111/j.1945-5100.2003.tb00027.x.
- Hood, L. L., P. J. Coleman Jr., and D. E. Wilhelm (1979), The Moon: Sources of the crustal magnetic anomalies, *Science*, *204*, 53–57, doi:10.1126/science.204.4388.53.
- Hood, L. L., A. Zakharian, J. Halekas, D. L. Mitchell, R. P. Lin, M. H. Acuña, and A. B. Binder (2001), Initial mapping and interpretation of lunar crustal magnetic anomalies using Lunar Prospector magnetometer data, *J. Geophys. Res.*, *106*, 27,825–27,840, doi:10.1029/2000JE001366.
- Kantelhardt, J. W. (2009), Fractal and multifractal time series, in *Encyclopedia of Complexity and Systems Science*, edited by R. A. Meyers, pp. 3754–3779, Springer, New York.
- Lawrence, K., C. Johnson, L. Tauxe, and J. Gee (2008), Lunar paleointensity measurements: Implications for lunar magnetic evolution, *Phys. Earth Planet. Inter.*, *168*, 71–87, doi:10.1016/j.pepi.2008.05.007.
- Lin, R. P. (1979), Constraints on the origins of lunar magnetism from electron reflection measurements of surface magnetic fields, *Phys. Earth Planet. Inter.*, *20*, 271–280, doi:10.1016/0031-9201(79)90050-5.
- Maus, S., and V. P. Dimri (1994), Scaling properties of potential fields due to scaling sources, *Geophys. Res. Lett.*, *21*, 891–894, doi:10.1029/94GL00771.
- Mitchell, D. L., J. S. Halekas, R. P. Lin, S. Frey, L. L. Hood, M. H. Acuña, and A. B. Binder (2008), Global mapping of lunar crustal magnetic fields by Lunar Prospector, *Icarus*, *194*, 401–409, doi:10.1016/j.icarus.2007.10.027.
- Pilkington, M., and J. P. Todoeschuck (1993), Fractal magnetization of continental crust, *Geophys. Res. Lett.*, *20*, 627–630, doi:10.1029/92GL03009.
- Purucker, M. E. (2008), A global model of the internal magnetic field of the Moon based on Lunar Prospector magnetometer observations, *Icarus*, *197*, 19–23, doi:10.1016/j.icarus.2008.03.016.
- R. A. Carley, Grant Institute of Earth Science, University of Edinburgh, Edinburgh EH9 3JW, UK.
- J. S. Halekas, R. J. Lillis, and R. P. Lin, Space Sciences Laboratory, 7 Gauss Way, University of California, Berkeley, CA 94720, USA. (jazzman@ssl.berkeley.edu)
- M. Manga, Department of Earth and Planetary Sciences, University of California, Berkeley, CA 94720, USA.
- M. E. Purucker, Planetary Geodynamics Laboratory, NASA Goddard Space Flight Center, Greenbelt, MD 20771, USA.